Ultrasonics - Sonochemistry 59 (2019) 104738

Contents lists available at ScienceDirect

Ultrasonics - Sonochemistry

journal homepage: www.elsevier.com/locate/ultson

Ultrasound-assisted method to improve the structure of CeO_2@polyprrole core-shell nanosphere and its photocatalytic reduction of hazardous Cr^{6+}

Vellaichamy Balakumar, Hyungjoo Kim, Ramalingam Manivannan, Hyorim Kim, Ji Won Ryu, Gisu Heo, Young-A. Son*

Department of Advanced Organic Materials Engineering, Chungnam National University, 220 Gung-dong, Yuseong-gu, Daejeon 305-764, South Korea

ARTICLE INFO

Keywords:
CeO_2@polyprrole
Core-shell nanosphere
Photocatalytic degradation
Hexavalent chromium
Reusability and stability

ABSTRACT

In this work, the CeO_2@polypyrrole (CeO_2@PPy) core-shell nanosphere has been synthesized via an ultra-sonication method using bath type (WUC-D22H, Daihan Scientific, Korea) and they are utilized for the photo-reduction of hazardous Cr^{6+} to benign Cr^{3+}. The ultrasonic frequency and power were 20 kHz and 100 W, respectively. The PPy shielded CeO_2 in aqueous solution could prevent the dissolution of CeO_2 and to improve the photocatalytic ability of CeO_2. X-ray diffraction was used to confirm the crystalline structure of as prepared CeO_2@PPy core-shell and FT-IR was used to identify the functional groups. The uniform sized core of PPy and shell of CeO_2 were observed by transition electron microscopy. The ultrasonic assisted synthesized CeO_2@PPy core-shell exhibits a narrow bandgap (UV-DRS) and good reduction efficiency with higher reusability and stability compared to pure CeO_2, PPy and mechanical mixing of CeO_2@PPy. Moreover, the synergistic effect of CeO_2 and PPy core-shell structure facilitate a higher electron transfer rate and prolong lifetime of photo-generated electron-hole pairs which can achieve good reduction rate of 98.6% within 30 min. In particular, the pH, catalyst, and Cr^{6+} concentration effects were optimized in photocatalytic reduction reactions. Meanwhile, this photocatalysis with fast and effective electron transfer mechanism for the Cr^{6+} reduction was elucidated. This method opens a new window for simple fabrication of conducting polymers-based metal oxide nano-composite towards wastewater remediation and beyond.

1. Introduction

In general, heavy metals are easily entered in aquatics environment which causing serious contamination and a toxic effect to human and animals [1]. Among the heavy metals, chromium (Cr) is customarily used in cement industries, leather tanning, paint formulation, etc [2]. Its high valent Cr^{6+} has been categorized as a group I human carcinogen by the IARC (International Agency for the Research on Cancer) and the WHO (World Health Organization) has assigned 0.05 mg/L as a limit of Cr^{6+} [3]. Therefore, the fast and efficient removal of Cr^{6+} in aquatic systems is still needed for environmental safety and analysis. Up to now, Cr^{6+} removal has been employed by various methods including adsorption [4], electrochemical precipitation [5], reverse osmosis [6], ion exchange [7], solvent extraction [8], catalytic reduction [1,3] and photocatalytic degradation [9–11]. Among them, photocatalytic method has been investigated as one of the efficient conversion of toxic to benign form of organic and inorganic pollutants. In past decades, many studies have been explored on the photocatalytic removal of environmental pollutant, Cr^{6+} [12–15]. But, the cost effective and efficient catalysts to remove Cr^{6+} still have been recognized as one of the tasks in the photocatalysis community. Nanoceria have been used for research in many fields including catalysis, electronic, medicine and optics. Besides, the 3.2 eV band gap of cerium oxide (CeO_2) have some limitations of its application in photocatalysis which is deficient light absorption, separation and fast recombination of electron-hole pairs [16,17]. To conquer the above problems, many researchers have been developed responses such as CeO_2 coupled with metals (Ag [18], Au [18], Pt [19], Pd [16], Fe [20] and Cu [21]), metal oxides (TiO_2 [9], Bi_2WO_6 [10], SnS_2 [11]), carbon based materials (graphene [22] and g-C_3N_4 [23]) and heteroatom (N [24]) to form nanocomposites. Interestingly, CeO_2 based heterogeneous catalyst attracted attention by showing robust and stable photocatalytic reduction of Cr^{6+} [25].

Recently, conducting polymers supported heterogeneous photocatalysts have been attracted worldwide attention due to their excellent energy production and conversion, environmental remediation and beyond. Among polymers, polypyrrole (PPy) has a good utilization efficiency of visible-light for photocatalysts due to π-conjugated electron system of PPy [26]. In addition, the high electron donors and

* Corresponding author.
E-mail address: yason@cnu.ac.kr (Y.-A. Son).

https://doi.org/10.1016/j.ultsonch.2019.104738
Received 13 April 2019; Received in revised form 12 August 2019; Accepted 18 August 2019
Available online 19 August 2019
1350-4177/

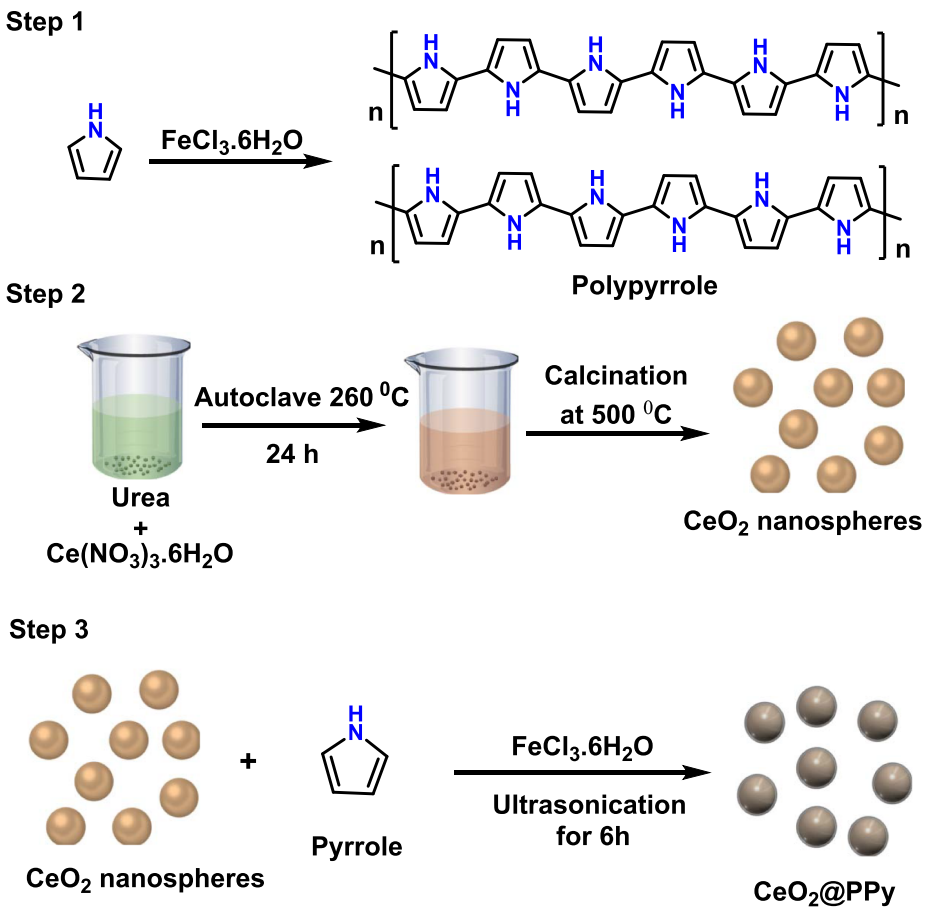

Scheme 1. Schematic representation of the CeO_2@PPy core-shell nanosphere synthesized through ultrasonic method.

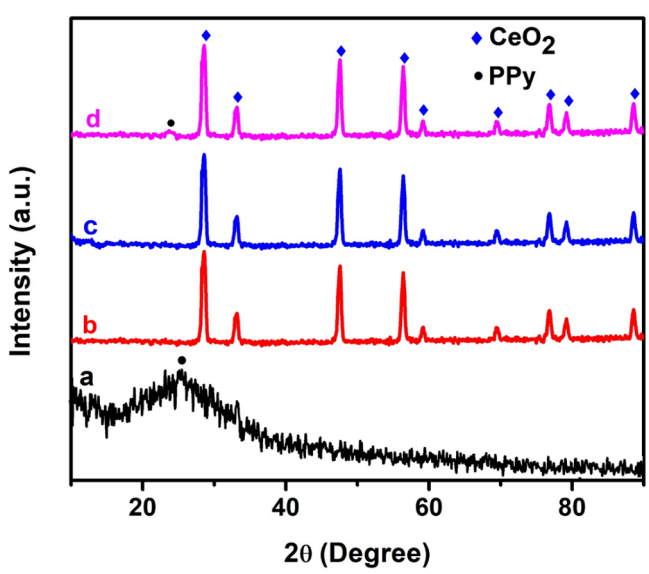

Fig. 1. XRD patterns of PPy (curve a), CeO_2 (curve b), CeO_2@PPy core-shell (curve c) synthesized via ultrasonic method and CeO_2@PPy (curve d) synthesized via mechanical mixing.

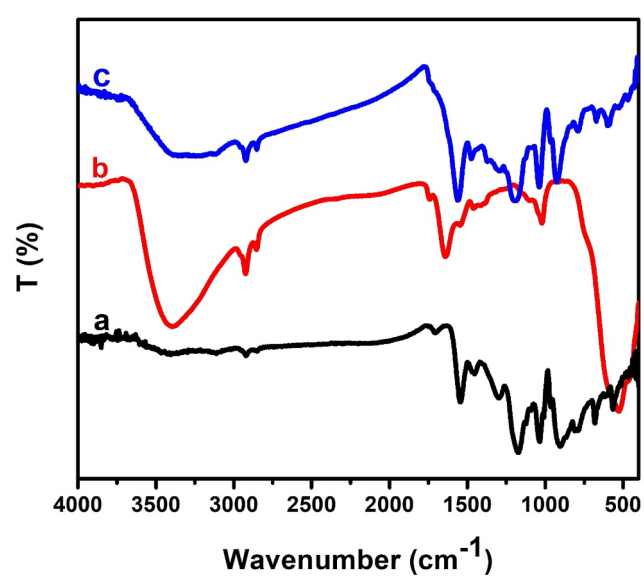

Fig. 2. FT-IR spectra of PPy (curve a), CeO_2 (curve b) and CeO_2@PPy core-shell nanosphere (curve c).

transporters properties can be achieved with the enhancement of the absorption capacity, charge separation and electron-hole pairs. Up to now, many researchers have used to PPy as active and reusable support for preparation of photocatalysts with good results. For example, L. K. Krehula et al. [27] have prepared PPy/TiO_2 nanocomposite to enhance the visible light active photocatalytic activity. F. A. Harraz et al. [28] have synthesized α-Fe_2O_3/PPy nanophotocatalyst to achieve a remarkable activity toward methylene blue degradation. L. Wang et al. [29] have studied near infrared light driven degradation of different organic pollutants by using PPy/$W_{18}O_{49}$ nanorods. J. Xu et al. [30] have reported an enhanced specific surface area of PPy-BiOI composite resulting in good adsorption and generation of more active sites to degrade organic pollutants. F. Duan et al. [31] used visible light active

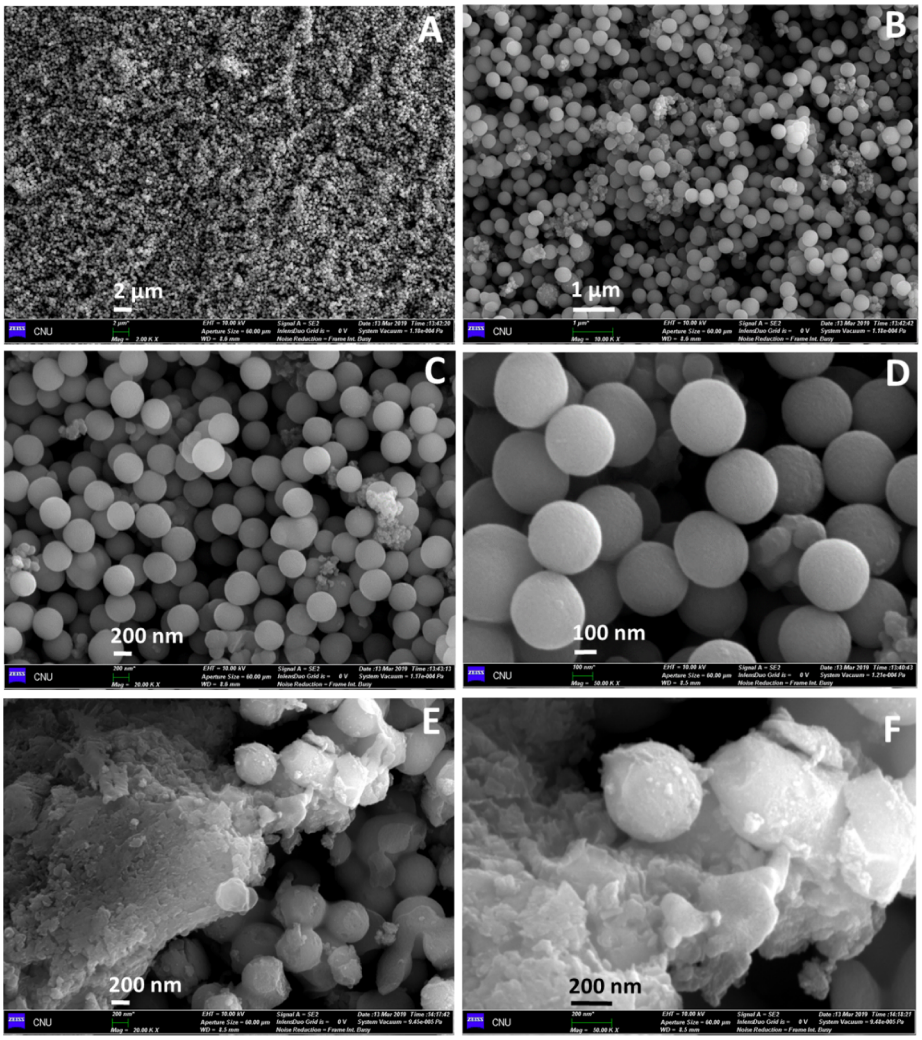

Fig. 3. (A–D) Different magnification SEM images of CeO_2@PPy core-shell nanosphere synthesized via ultrasonic method and (E&F) Different magnification SEM images of CeO_2@PPy synthesized via mechanical mixing.

PPY/Bi_2WO_6 nanocomposite for photoreduction of rhodamine-B and methylene blue in aqueous solution.

Compare to conventional methods, a rapid, economic and environmental friendly ultrasound-assisted method is used to develop nanocomposites with controlled size, morphology, phase purity and uniform distribution of particles on supportive surfaces [12,17,32,33]. A positive effect of ultrasound has enhanced the photocatalytic performance because of uniform distribution of particles by enhancing the surface-active sites for degradation process. Recently, modification of $Bi_2Sn_2O_7$-C_3N_4/Y nanophotocatalyst with various ratios of zeolite have shown good photocatalytic activity towards tetracycline [34]. Sonoprecipitation dispersion of ZnO nanoparticles over graphene oxide nanocomposite enhanced the photocatalytic reactivity and stability influenced by irradiation time and power [35]. Sonocatalytic degradation of a textile dye using CeO_2-biochar nanocomposite are some examples of ultrasound irradiation used to improve the photocatalyst performance [17].

Herein we report on a novel and stable of CeO_2@polypyrrole core-shell nanosphere photocatalyst has been synthesized via ultrasonic method. The synthesized core-shell photocatalyst demonstrated that The CeO_2 core is not dissolved in aqueous solution because shell of PPy could prevent the dissolution. Therefore, the CeO_2@PPy enhancing the structural stability. The core-shell of CeO_2@PPy nanospere exhibits a good visible light active photocatalytic detoxification activity and stability than pure CeO_2 and PPy. Finally, the efficient charge separation mechanism and stability of the nanocomposite has been demonstrated and investigated in detail. The proposed photocatalytic mechanisms are likely to a new window for the fabrication of conducting polymers-based metal oxide nanocomposite for wastewater remediation and beyond.

2. Experimental sections

2.1. Materials

In this work, all of the reagents were purchased from analytical grade and used directly without further purification. Pyrrole, cerium (III) nitrate hexahydrate ($Ce(NO_3)_3{\cdot}6H_2O$, 99%) and urea were purchased from Sigma–Aldrich, South Korea.

2.2. Synthesis of CeO_2 nanosphere

0.5 g of $Ce(NO_3)_3{\cdot}6H_2O$ were dispersed in 10 ml deionized water and 12 g of urea were dissolved in 40 ml of water and then the dissolved urea was transferred in to the above solution slowly. The resultant solution was then transferred to an autoclave vessel, heated to 260 °C, and

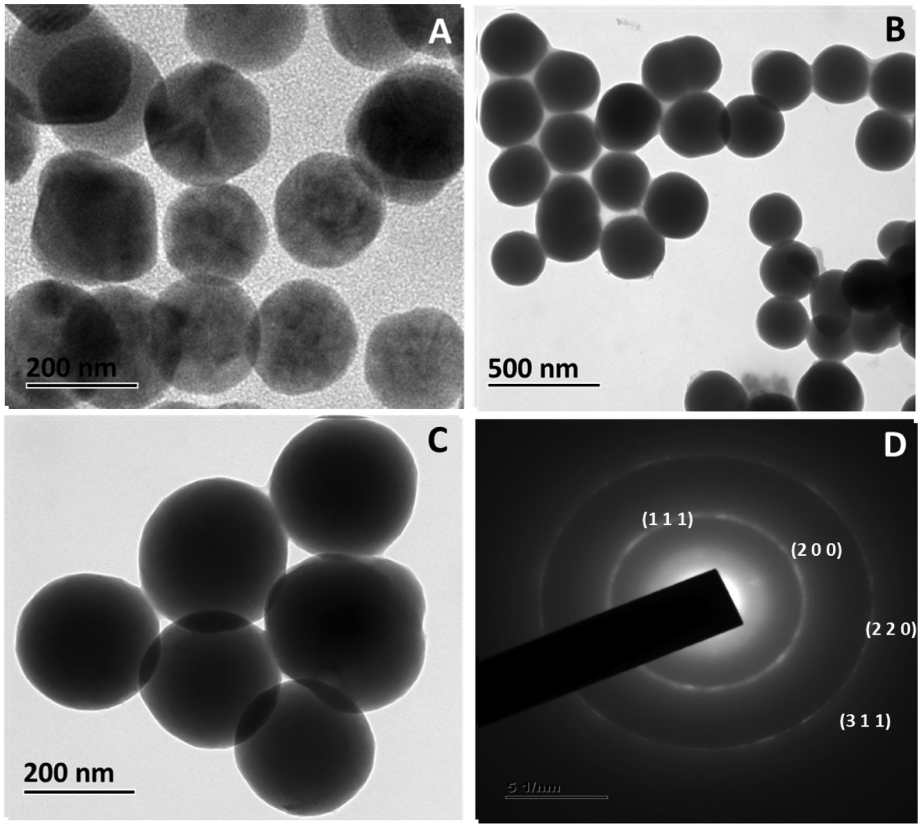

Fig. 4. (A) TEM image of CeO_2, (B&C) different magnification TEM images of CeO_2@PPy core-shell nanosphere and (D) SAED pattern of CeO_2@PPy core-shell nanosphere.

maintained at this temperature for 24 h. The obtained samples were collected and washed with water and ethanol in twice. Then, it was dried at air oven and subjected to calcination for 2 h at 500 °C to get the final product.

2.3. Synthesis of CeO_2@PPy core-shell nanosphere

0.2 g of synthesized CeO_2 and 0.5 ml of pyrrole were dispersed in 25 ml deionized water and 1.5 g $FeCl_3$ (1:1.25 pyrrole: $FeCl_3$ ratio) was dispersed into 25 ml of 1 M methanesulphonic acid. The resulting second solution was dropwise transferred in to the aqueous solution pyrrole and CeO_2. After that the solution was ultra-sonicated for 6 h (irradiation power 100 W). Then it was filtered, washed, and dried at 110 °C for 12 h. The same reaction was also carried out using simple mechanical mixing and compare the results. Pure polypyrrole was prepared by the same procedure (ultrasonication) without adding CeO_2 nanosphere. The preparation process of PPy, CeO_2 and core-shell nanosphere of CeO_2@PPy are shown in Scheme 1.

2.4. Instrumentations

The UV–DRS spectra were used to record the absorption value of samples on a Shimadzu Solid Spec-2700 instrument using $BaSO_4$ as the reference. Infrared spectra experiments were collected on ALPHA-P spectrometer. The XRD measurements were performed on a Cu Kα radiation (λ = 1.54056 Å) using (PHILIPS, X'Pert-MPD System, Max P/N: 3 kW/40 kV, 45 Ma, Netherlands). For SEM analysis were carried at LYRA3 XMU. High-resolution surface structure and selected area electron diffraction (SAED) were obtained with a transmission electron microscope (TEM, FEI TECNAI T20 G2) operating at 100 kV. Finally, HEBER immersion type photoreactor (HIPR-MP125) were used to perform photocatalytic experiments.

2.5. Photocatalytic measurements

The photo-reduction ability of CeO_2@PPy were evaluated towards Cr^{6+} under visible light irradiation (λ > 450 nm) at 30 °C and the average light intensity is found to be 29.36 W/m^{-2}. In a standard experiment, 100 ml aqueous solution of Cr^{6+} (0.1 mM) which was prepared from $K_2Cr_2O_7$ and 50 mg of catalysts was added in to the above aqueous Cr^{6+} solution. Then, the suspension was stirred under dark conditions for 30 min to ensure the adsorption-desorption equilibrium. During the irradiation, the solution (5 ml) were taken at every 5 min and centrifuged at 1000 rpm and measured UV–visible absorbance spectroscopy. After completing the reduction process, the catalyst was separated and it was used to carry out the next catalytic reduction process of fresh substrates. The reduction percentage was calculated using ($C_0 - C_t/C_0 \times 100$) where, C_t and C_0 are the instantaneous concentration of Cr^{6+} at time t and initial concentration of Cr^{6+} respectively.

3. Result and discussions

3.1. Structural characterization

XRD was analyzed to determine the crystalline structure of PPy, CeO_2 and CeO_2@PPy core-shell nanocomposite. XRD pattern shows a broad peak appears at around 24.21° which is corresponding to the

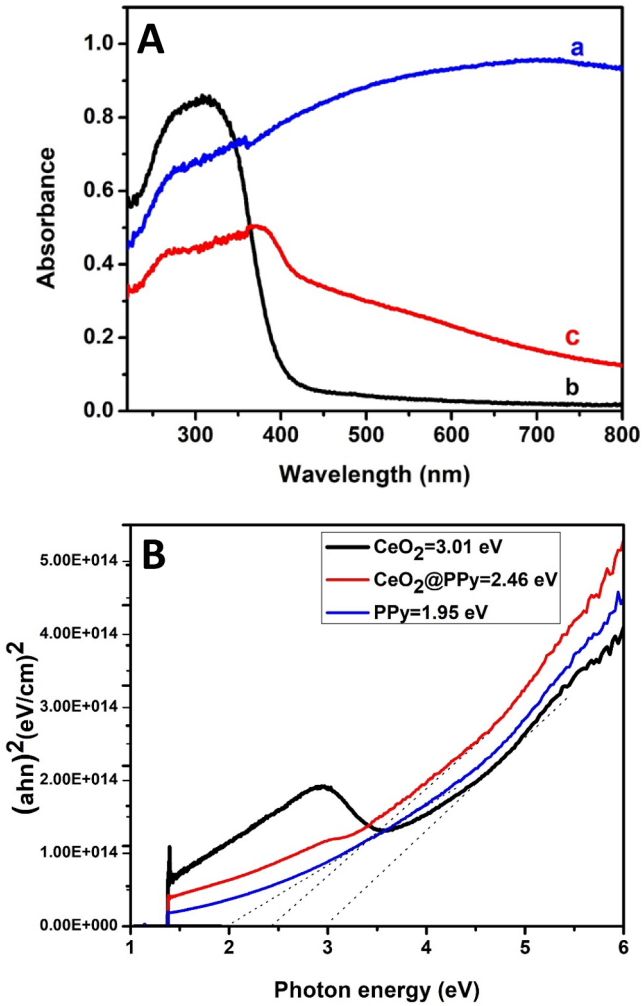

Fig. 5. (A) UV–visible diffuse absorption spectra of the PPy (curve a), CeO_2 (curve b) and CeO_2@PPy core-shell nanosphere (curve c) and (B) Tauc's plots of PPy (blue line), CeO_2 (black line) and CeO_2@PPy core-shell nanosphere (red line).

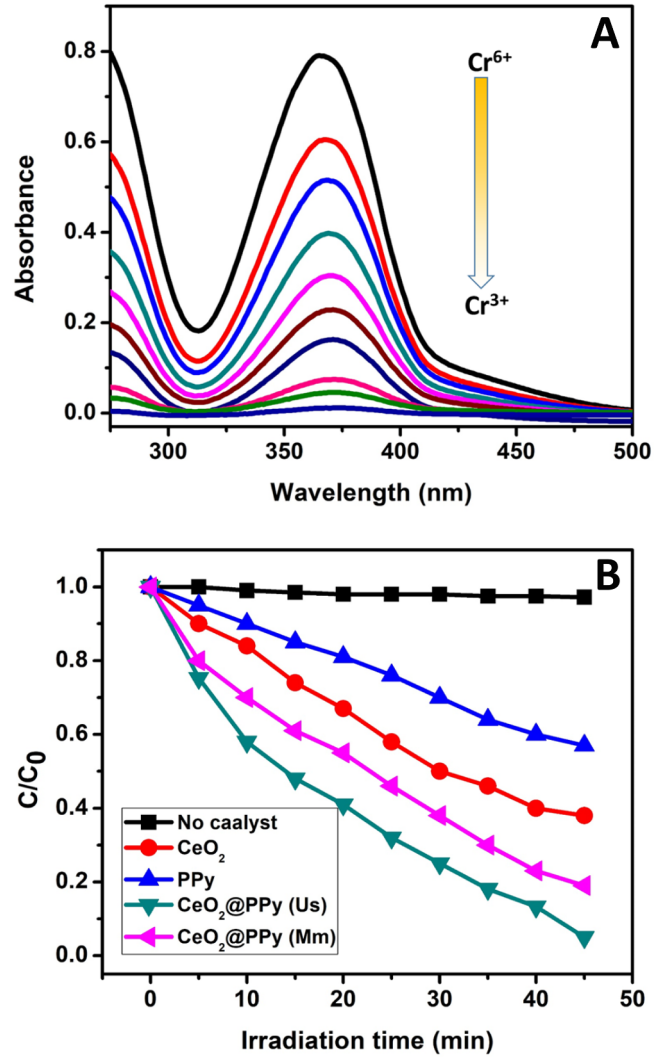

Fig. 6. (A) Photocatalytic reduction of Cr^{6+} to Cr^{3+} in the presence of CeO_2@PPy core-shell nanosphere and (B) Photocatalytic Cr^{6+} reduction curves of C/C_0 vs time.

amorphous nature of pure PPy as shown in Fig. 1 (curve a). Pure CeO_2 was observed at cubic fluorite structure of diffraction peaks indexed (JCPDS no. 34-0394). This phase diffraction peaks observed at 28.66°, 33.09°, 47.52°, 56.40°, 59.05°, 69.45°, 76.78°, 79.20° and 88.57° (Fig. 1 (curve b)) correspond to (1 1 1), (2 0 0), (2 2 0), (3 1 1), (2 2 2), (4 0 0), (3 3 1), (4 2 0), and (4 2 2) planes for CeO_2, respectively [36]. The average crystallite size of CeO_2 was calculated, resulting in about 197.2 nm from (1 1 1) peak of XRD using Debye-Scherrer equation [37]. Compared with bare CeO_2, the XRD patterns of CeO_2@PPy core shell (curve c) nanosphere (ultrasonic synthesis) did not affect the reflections of CeO_2 nanoparticles indicating that crystal structure of CeO_2 core was not affected by PPy shell. Moreover, PPy diffraction peaks are invisible in the CeO_2@PPy, which is due to the low concentration and crystallinity of PPy. Compared to this method, mechanical mixing method synthesized CeO_2@PPy exhibits a new peak at 24° which indicates the PPy. Herein we concluded that mechanical mixing method synthesized CeO_2@PPy was not formed in core-shell, which is confirmed by SEM images.

Fig. 2 shows the FT-IR spectra of PPy, CeO_2 and core-shell structure of CeO_2@PPy nanocomposite photocatalysts. As can be seen in Fig. 2 (curve a) pure PPy has display bands at 3405, 1711, 1548, 1461 and 1177 cm^{-1}. The peak observed at 3405 cm^{-1} is attributed to —NH stretching vibration of PPy while the peaks at 1711 and 1548 cm^{-1} are represent to C—C ring stretching and C═C backbone stretching, respectively [26]. The PPy, C—H in-plane and C—N stretching vibrations are observed at 1461 and 1177 cm^{-1} [29]. For pure CeO_2, (Fig. 2 (curve b)) peaks at 522, 1027, 1647 and 3402 cm^{-1} with all absorption peaks appeared in proper position which is good agreement with earlier reported results [38]. It can be seen that the FT-IR spectra of CeO_2@PPy (Fig. 2 (curve b)) photocatalysts, the intensity of both PPy and CeO_2 peaks decreases because PPy was coated on the shell of CeO_2.

Fig. 3A–D different magnification SEM images of CeO_2@PPy has core-shell nanosphere showing that average particles size was 200 nm. As shown in Fig. 3E &F, the mechanical mixing method to synthesize CeO_2@PPy was not formed in core-shell. TEM study were used to find out the size and shape of the as-prepared CeO_2 and core-shell structure of CeO_2@PPy. As shown in Fig. 4A, the uniform sized nanospheres and the average diameter was found to be 200 nm of CeO_2 particles. Further, the core-shell structure CeO_2@PPy has been given in Fig. 4B&C. It

Table 1
Photocatalytic activity of different CeO_2 based catalysts for the photo-reduction of Cr^{6+}.

Materials	Catalyst weight (mg)	Cr Concentration	Time (min)	Efficiency (%)	Catalyst stability cycles	Ref.
CeO_2-TiO_2	50	2 mM	180	99.6	3	9
CeO_2@Bi_2WO_6	20	8 mg/L	60	99.6	–	10
CeO_2/SnS_2	300	50 mg/L	80	–	5	11
Pd/CeO_2/g-C_3N_4	50	0.1 mM	40	–	4	25
CeO_2@Pt@TiO_2	30	5.0 mg/L	150	99.0	–	40
CeO_2-QDs/BiOX	50	20 mg/L	60	97.0	6	41
Y-CeO_2/PCN	120	100 mg/mL	240	98.1	–	42
CeO_2@PPy	10	0.1 mM	45	98.6	5	This work

can be seen clearly that the outside of the as-prepared CeO_2 particles surface was uniformly coated with PPy shell showing distinctly different from the CeO_2 core. The SAED lattice fringes of CeO_2@PPy core-shell nanosphere exhibited a spacing of 0.27 nm (Fig. 4D), which is in good agreement with the XRD results.

Diffuse reflectance spectroscopy is used to measure the optical absorption property of the PPy, CeO_2 and core-shell structure of CeO_2@PPy nanosphere as hown in Fig. 5A. The pure PPy showed the characteristic absorption edge at about 500 nm as shown in Fig. 4a (curve a). The pure CeO_2 light absorption peak was observed at 310 nm (Fig. 5A (curve b)) and the corresponding to a band gap (Eg) of 3.01 eV [25,38] due to electron transition from oxygen to cerium [39]. When PPy shell was coated on the surface of CeO_2 core (Fig. 5A (curve C)), optical absorption was enhanced to the range of the visible region compared to pure CeO_2, resulting from the PPy. The Tauc's equation was used to determine the band gap energy of PPy, CeO_2 and CeO_2@PPy core-shell nanosphere and the graph plotted $(\alpha h\nu)^2$ against the photon energy ($h\nu$). The band gap values were found to be 1.95 (PPy), 3.01 (CeO_2) and 2.46 Ev (CeO_2@PPy) in Fig. 5B.

3.2. Photocatalytic detoxification of Cr^{6+}

In Fig. 6A, the photocatalytic activities of PPy, CeO_2 and CeO_2@PPy were described, showing the reduction of hexavalent chromium to trivalent chromium under the visible light. The Cr^{6+} photolytic degradation was negligible in the absence of the catalyst. The Cr^{6+} degradation in the presence of pure PPy and CeO_2 were investigated and the results showed slightly degradation (48 and 69%, respectively) as shown in Fig. 6B. In contrast, nearly 100% of Cr^{6+} was degraded with (30 min) irradiation in the presence of CeO_2@PPy photocatalyst under the same conditions. As shown in Fig. 6A, the absorption peak intensity of Cr^{6+} ions were drastically decreased and finally disappear as much as irradiation time increased [25]. Complete reduction of toxic Cr^{6+} to Cr^{3+} was clearly observed within 30 min. Also the yellow color of Cr^{6+} was changed to colorless, indicating the reduction of hazard Cr^{6+} to benign Cr^{3+}. These results indicated that core-shell CeO_2@PPy photocatalyst is obviously superior to pure CeO_2 and PPy as well as mechanical mixing of CeO_2@PPy. The Cr^{6+} reduction rate constant k of photocatalysts was evaluated by ln (C_0/C_t) against t, showing that the value for PPy, CeO_2 and CeO_2@PPy core-shell are found to be 0.0012, 0.0097 and 0.0639 min^{-1}, respectively. The CeO_2@PPy core-shell is compared with other reported CeO_2 based photocatalysts for the reduction of Cr^{6+} in Table 1. [40,10,41,9,11,25,42].

3.3. Optimization of various parameters

In various pH (pH 2, 5, 7 and 9), the Cr^{6+} degradation efficiency was studied by fixing other parameters (catalyst weight, Cr^{6+} concentration) constant as shown in Fig. 7A. This figure can clearly show that the maximum detoxification of Cr^{6+} was observed in acid solution. In acidic pH the catalyst surface can create positively charges and Cr^{6+} gets negative charged species ($HCrO_4^-$ and $Cr_2O_7^{2-}$), leading to strong adsorption of Cr^{6+} on the catalyst surface, consequently increase to photocatalytic reduction rate [1,14]. On the other hand, in higher pH, the catalyst surface became negatively charged, which repels Cr^{6+} species and the conversion products of Cr^{3+} can be easily precipitated in basic conditions [43]. According to this, the amount of Cr^{6+} absorption and rate of reduction efficiency was achieved at lower pH.

In order to find an optimum dosage of the CeO_2@PPy core-shell, the pH and Cr^{6+} concentration was kept constant and the amount of catalyst varying from 0.5, 1.0 and 1.5 mg were tested. In addition, the degradation percentage was calculated as shown in Fig. 7B. According to the results, it can be seen that 1.0 mg of the catalyst loaded solution has been achieved higher photocatalytic detoxification. Moreover, lower or higher amount of catalyst loaded solutions had poor activity because of fewer active sites and solar light inhibition in solution, respectively [44,45]. These are the reasons to reduce the degradation percentage.

Fig. 7C shows the effect of Cr^{6+} initial concentration on detoxification using CeO_2@PPy core-shell under visible light irradiation. The good degradation percentage (98.2%) were achieved in the initial concentration of Cr^{6+}. It was clearly observed that the enhancement of Cr^{6+} concentration reduce the rate of conversion since the higher Cr^{6+} prevents light on the catalyst with the reduction of generation for electrons and hole-pairs [45,46]. Furthermore, the minimum concentration of Cr^{6+} completely adsorbed on to the catalyst surface and generation of active species increases leading to the enhancement of the conversion percentage.

3.4. Possible charge separation and degradation mechanism

Based on the experimental analysis above, a charge separation and Cr^{6+} degradation mechanism of CeO_2@PPy nanospheres has been proposed in Fig. 8. It was well-known that both PPy and CeO_2 can generate electrons and holes under visible light irradiation. The generated electrons migrated from HOMO of PPy and VB of CeO_2 to LOMO of PPy and CB of CeO_2 respectively. Further, the LUMO of PPy electrons can be directly injected into the CB of CeO_2. However, the LUMO potential of PPy is more negative than CB of CeO_2. Finally, the gathered electrons in CB of CeO_2 can react with surface adsorbed oxygen molecules to generate super oxide radical anions [38,47,48]. Simultaneously, the excited holes produced by CeO_2 are injected into the HOMO of PPy due to the difference in valence band edge potentials and then it was reacted with water molecules to generate hydroxide radicals [49]. These generated super oxide radical anions and hydroxide radicals are easily degrading the adsorbed contaminants. Obviously, the upgrading of photocatalytic activity induced by the synergistic effect of CeO_2 and PPy had efficient charge separation and reduce the rate of recombination.

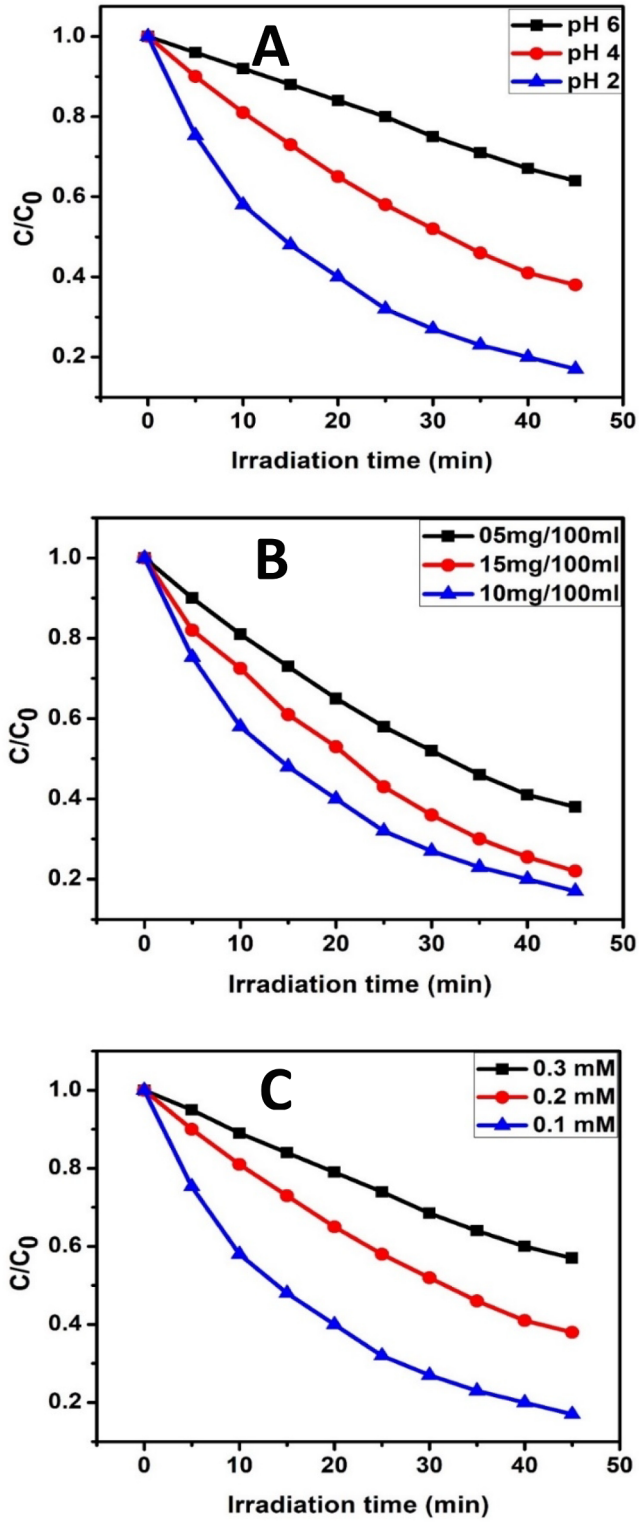

Fig. 7. (A) Effect of pH (B) catalyst dotage and (C) Cr^{6+} concentrations.

3.5. Stability and reusability

To identify the stability and reusability of the CeO_2@PPy core-shell were evaluated in Fig. 9. The reduction of Cr^{6+} has been achieved above 97% even after five catalytic cycles. The slight loss of efficiency can be attributed to unavoidable loss of catalyst mass or blocking of surface of the catalyst by degraded product. Further, XRD and SEM analysis (Fig. 10A&B) of after five recyclable catalyst was observed no noticeable changes. Therefore, ultrasound-assisted synthesis is a useful method for improvement of degradation efficiency and catalyst stability.

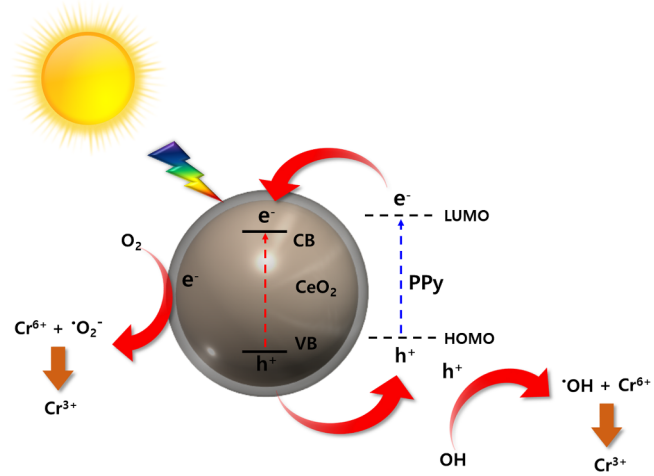

Fig. 8. CeO_2@PPy core-shell nanosphere fast and efficient electron transfer mechanism for the reduction of toxic Cr^{6+}.

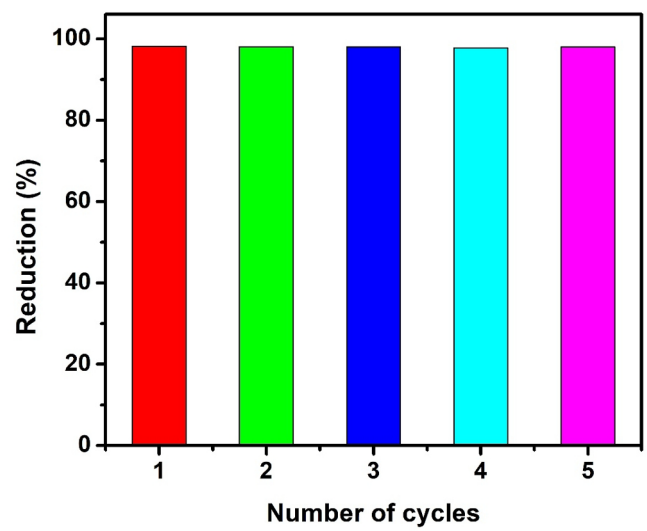

Fig. 9. The repeated photocatalytic reduction experiments using CeO_2@PPy core-shell nanosphere photocatalyst.

4. Conclusions

In this paper, CeO_2@PPy core-shell structure of photocatalyst has been synthesized via ultrasound-assisted method and the resulting samples were compared to mechanical mixing preparation. As observed that ultrasound irradiation improves the uniform distribution of particles and formation of core of CeO_2 and PPy shell. The ultrasonic assisted synthesis of CeO_2@PPy exhibits a narrow bandgap and good reduction efficiency compared to pure CeO_2 and PPy. The synergistic CeO_2 and PPy core-shell structure facilitate a higher electron transfer rate and prolong lifetime of photogenerated electron-hole pairs which could achieve good reduction rate of 98.6% within 30 min. Obviously, the ultrasound irradiation has a positive effect on photocatalysts synthesis and reduction of hazardous Cr^{6+} to benign Cr^{3+} in aqueous solutions. This method opens a new window for simple fabrication of conducting polymers-based metal oxide nanocomposite towards wastewater remediation and beyond.

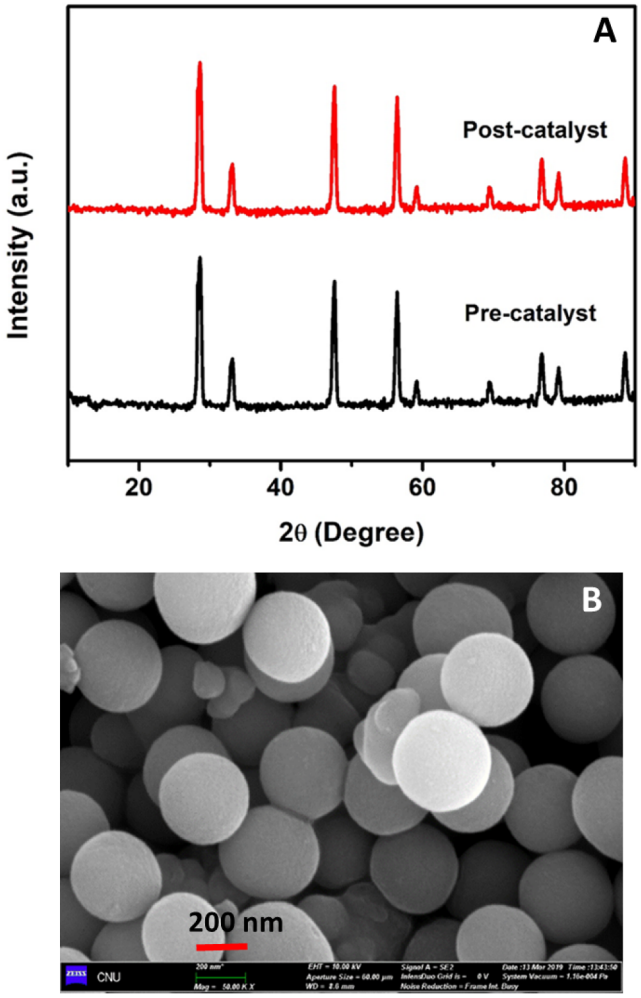

Fig. 10. XRD patterns of pre- and post- CeO_2@PPy core-shell nanosphere and (B) SEM image of CeO_2@PPy core-shell nanosphere photocatalyst.

Acknowledgements

This study was supported by the Basic Science Research Program through the National Research Foundation of Korea (NRF) funded by the Ministry of Science, ICT and Future Planning (Grant No. NRF-2017R1E1A1A01074266). This work was supported by the Industrial Fundamental Technology Development Program (10076350) funded by the Ministry of Trade, Industry and Energy (MOTIE) of Korea.

References

[1] B. Vellaichamy, P. Periakaruppan, B. Nagulan, Reduction of Cr^{6+} from wastewater using a novel in situ-synthesized PANI/MnO_2/TiO_2 nanocomposite: renewable, selective, stable, and synergistic catalysis, ACS Sustain. Chem. Eng. 5 (2017) 9313–9324.
[2] A. Dandapat, D. Jana, G. De, Pd nanoparticles supported mesoporous γ-Al_2O_3 film as a reusable catalyst for reduction of toxic Cr^{VI} to Cr^{III} in aqueous solution, Appl. Catal. A 396 (2011) 34–39.
[3] B. Vellaichamy, P. Periakaruppan, A facile, one-pot and eco-friendly synthesis of gold/silver nanobimetallics smartened rGO for enhanced catalytic reduction of hexavalent chromium, RSC Adv. 6 (2016) 57380–57388.
[4] J. Sun, Z. Zhang, J. Ji, M. Dou, F. Wang, Removal of Cr^{6+} from wastewater via adsorption with high-specific-surface-area nitrogen-doped hierarchical porous carbon derived from silkworm cocoon, Appl. Surf. Sci. 405 (2017) 372–379.
[5] N. Kongsricharoern, C. Polprasert, Electrochemical precipitation of chromium (Cr^{6+}) from an electroplating wastewater, Water Sci. Tech. 31 (1995) 109–117.
[6] K. Chon, S.J. Kim, J. Moon, J. Cho, Combined coagulation-disk filtration process as a pretreatment of ultrafiltration and reverse osmosis membrane for wastewater reclamation: an autopsy study of a pilot plant, Water Res. 46 (2012) 1803–1816.
[7] H. Mekatel, S. Amokrane, A. Benturki, D. Nibou, Treatment of polluted pqueous solutions by Ni^{2+}, Pb^{2+}, Zn^{2+}, Cr^{+6}, Cd^{+2} and Co^{+2} ions by ion exchange process using faujasite zeolite, Procedia Eng. 33 (2012) 52–57.
[8] M.A. Elbagermi, A.I. Alajtal, H.G.M. Edwards, Spectrophotometric determination of chromium (VI) in nitric acid by means of solvent extraction with molten mixtures of naphthalene and biphenyl, APCBEE Procedia 5 (2013) 378–382.
[9] H. Jiang, M. Li, J. Liu, X. Li, L. Tian, P. Chen, Alkali-free synthesis of a novel heterostructured CeO_2-TiO_2 nanocomposite with high performance to reduce Cr(VI) under visible light, Ceram. Int. 44 (2018) 2709–2717.
[10] Z. Lv, H. Zhou, H. Liu, B. Liu, M. Liang, H. Guo, Controlled assemble of oxygen vacant CeO_2@Bi_2WO_6 hollow magnetic microcapsule heterostructures for visible-light photocatalytic activity, Chem. Eng. J. 330 (2017) 1297–1305.
[11] C. Hou, Y. Zhang, J. Li, A. Zhu, In-situ hydrothermal synthesis of CeO_2/SnS_2 heterojunction for use as a new efficient visible-light-driven photocatalyst, Mater. Lett. 213 (2018) 154–157.
[12] P. Wang, W. Ji, M. Li, G. Zhang, J. Wang, $Bi_{25}VO_{40}$ microcube with step surface for visible light photocatalytic reduction of Cr(VI): enhanced activity and ultrasound assisted regeneration, Ultrason. Sonochem. 38 (2017) 289–297.
[13] S.L. Prabavathi, P.S. Kumar, K. Saravanakumar, V. Muthuraj, S. Karuthapandian, A novel sulphur decorated 1-D MoO_3 nanorods: facile synthesis and high performance for photocatalytic reduction of hexavalent chromium, J. Photochem. Photobiol. A 356 (2018) 642–651.
[14] L. Zhang, C.-G. Niu, C. Liang, X.-J. Wen, D.-W. Huang, H. Guo, X-F. Zhao, G-M. Zeng, One-step in situ synthesis of CdS/SnO_2 heterostructure with excellent photocatalytic performance for Cr(VI) reduction and tetracycline degradation, Chem. Eng. J. 352 (2018) 863–875.
[15] M. Abinaya, K. Saravanakumar, E. Jeyabharathi, V. Muthuraj, Synthesis and characterization of 1D-MoO_3 nanorods using *Abutilon indicum* extract for the photoreduction of hexavalent chromium, J. Inorg. Organomet. Polym. Mater. 29 (2019) 101–110.
[16] D. Channei, A. Nakaruk, P. Jannoey, S. Phanichphant, Preparation and characterization of Pd modified CeO_2 nanoparticles for photocatalytic degradation of dye, Solid State Sci. 87 (2019) 9–14.
[17] A. Khataee, P. Gholami, D. Kalderis, E. Pachatouridou, M. Konsolakis, Preparation of novel CeO_2-biochar nanocomposite for sonocatalytic degradation of a textile dye, Ultrason. Sonochem. 41 (2018) 503–513.
[18] M. Mittal, A. Gupta, O.P. Pandey, Role of oxygen vacancies in Ag/Au doped CeO_2 nanoparticles for fast photocatalysis, Sol. Energy 165 (2018) 206–216.
[19] N. Zhang, X. Fu, Y.-J. Xu, A facile and green approach to synthesize Pt@CeO_2 nanocomposite with tunable core-shell and yolk-shell structure and its application as a visible light photocatalyst, J. Mater. Chem. 21 (2011) 8152–8158.
[20] D. Channei, B. Inceesungvorn, N. Wetchakun, S. Ukritnukun, A. Nattestad, J. Chen, S. Phanichphant, Photocatalytic degradation of methyl orange by CeO_2 and Fe–doped CeO_2 films under visible light irradiation, Sci. Rep. 4 (2014) 5757.
[21] K.S. Ranjith, C.-L. Dong, Y.-R. Lu, Y.-C. Huang, C.-L. Chen, P. Saravanan, K. Asokan, R.T. Rajendra Kumar, Evolution of visible photocatalytic properties of Cu-doped CeO_2 nanoparticles: role of Cu^{2+}-mediated oxygen vacancies and the mixed-valence states of Ce ions, ACS Sustainable, Chem. Eng. 67 (2018) 8536–8546.
[22] A. Murali, Y.P. Lan, P.K. Sarswat, M.L. Free, Synthesis of CeO_2/reduced graphene oxide nanocomposite for electrochemical determination of ascorbic acid and dopamine and for photocatalytic applications, Mater. Today Chem. 12 (2019) 222–232.
[23] X. She, H. Xu, H. Wang, J. Xia, Y. Song, J. Yan, Y. Xu, Q. Zhang, D. Du, H. Li, Controllable synthesis of CeO_2/g-C_3N_4 composites and their applications in the environment, Dalton Trans. 44 (2015) 7021–7031.
[24] C. Wu, Solvothermal synthesis of N-doped CeO_2 microspheres with visible light-driven photocatalytic activity, Mater. Lett. 139 (2015) 382–384.
[25] K. Saravanakumar, R. Karthik, S.-M. Chen, J. Vinoth Kumar, K. Prakash, V. Muthuraj, Construction of novel Pd/CeO_2/g-C_3N_4 nanocomposites as efficient visible-light photocatalysts for hexavalent chromium detoxification, J. Colloid Interface Sci. 504 (2017) 514–526.
[26] B. Vellaichamy, P. Periakaruppan, R. Arumugam, K. Sellamuthu, B. Nagulan, A novel photocatalytically active mesoporous metal-free PPy grafted MWCNT nanocomposite, J. Colloid Interface Sci. 514 (2018) 376–385.
[27] L.K. Krehula, J. Stjepanović, M. Perlog, S. Krehula, V. Gilja, J. Travas-Sejdic, Z. Hrnjak-Murgić, Conducting polymer polypyrrole and titanium dioxide nanocomposites for photocatalysis of RR45 dye under visible light, Polym. Bull. 76 (2019) 1697–1715.
[28] Farid A. Harraz, Adel A. Ismail, S.A. Al-Sayari, A. Al-Hajry, Novel α-Fe_2O_3/polypyrrole nanocomposite with enhanced photocatalytic performance, J. Photochem. 299 (2015) 18–24.
[29] L. Wang, S. Jiao, C. Li, Y. Qu, B. Wang, Promoting infrared light driven photocatalytic activity of $W_{18}O_{49}$ nanorods by coupling polypyrrole, Res. Chem. Intermed. 44 (2018) 5455–5466.
[30] J. Xu, Y. Hu, C. Zeng, Y. Zhang, H. Huang, Polypyrrole decorated BiOI nanosheets: efficient photocatalytic activity for treating diverse contaminants and the critical role of bifunctional polypyrrole, J. Colloid Interface Sci. 505 (2017) 719–727.
[31] F. Duan, Q. Zhang, D. Shi, M. Chen, Enhanced visible light photocatalytic activity of Bi_2WO_6 via modification with polypyrrole, Appl. Surf. Sci. 268 (2013) 129–135.
[32] M. Stucchi, G. Cerrato, C.L. Bianchi, Ultrasound to improve both synthesis and pollutants degradation based on metal nanoparticles supported on TiO_2, Ultrason. Sonochem. 51 (2019) 462–468.
[33] S. Mallakpour, S. Shamsaddinimotlagh, Ultrasonic-promoted rapid preparation of PVC/TiO_2-BSA nanocomposites: characterization and photocatalytic degradation of methylene blue, Ultrason. Sonochem. 41 (2018) 361–374.
[34] S. Heidari, M. Haghighi, M. Shabani, Ultrasound assisted dispersion of $Bi_2Sn_2O_7$-C_3N_4 nanophotocatalyst over various amount of zeolite Y for enhanced solar-light photocatalytic degradation of tetracycline in aqueous solution, Ultrason. Sonochem.

43 (2018) 61–72.
[35] M. Zarrabi, M. Haghighi, R. Alizadeh, Sonoprecipitation dispersion of ZnO nanoparticles over graphene oxide used in photocatalytic degradation of methylene blue in aqueous solution: influence of irradiation time and power, Ultrason. Sonochem. 48 (2018) 370–382.
[36] R. Magudieshwaran, J. Ishii, K.C.N. Raja, C. Terashima, R. Venkatachalam, A. Fujishima, S. Pitchaimuthu, Green and chemical synthesized CeO_2 nanoparticles for photocatalytic indoor air pollutant degradation, Mater. Lett. 239 (2019) 40–44.
[37] B. Vellaichamy, P. Periakaruppan, Ag nanoshell catalyzed dedying of industrial effluents, RSC Adv. 6 (2016) 31653–31660.
[38] K. Saravanakumar, M.M. Ramjan, P. Suresh, V. Muthuraj, Fabrication of highly efficient visible light driven Ag/CeO_2 photocatalyst for degradation of organic pollutants, J. Alloys Compd. 664 (2016) 149–160.
[39] S. Li, J. Cai, X. Wu, B. Liu, Q. Chen, Y. Li, F. Zheng, TiO_2@Pt@CeO_2 nanocomposite as a bifunctional catalyst for enhancing photo-reduction of Cr (VI) and photo-oxidation of benzyl alcohol, J. Hazard. Mater. 346 (2018) 52–61.
[40] J. Yang, Y. Liang, K. Li, G. Yang, S. Yin, One-step low-temperature synthesis of 0D CeO_2 quantum dots/2D BiOX (X = Cl, Br) nanoplates heterojunctions for highly boosting photo-oxidation and reduction ability, Appl. Catal. B: Environ. 250 (2019) 17–30.
[41] H. Yang, B. Xu, S. Yuan, Q. Zhang, M. Zhang, T. Ohno, Synthesis of Y-doped CeO_2/PCN nanocomposited photocatalyst with promoted photoredox performance, Appl. Catal. B: Environ. 243 (2019) 513–521.
[42] S. Tsunekawa, R. Sahara, Y. Kawazoe, Y. Kawazoe, Origin of the blue shift in ultraviolet absorption spectra of nanocrystalline CeO_{2-x} particles, Mater. Trans. JIM 41 (2000) 1104–1107.
[43] Q. Wu, J. Zhao, G. Qin, C. Wang, X. Tong, S. Xue, Photocatalytic reduction of Cr(VI) with TiO_2 film under visible light, Appl. Catal. B: Environ. 142–143 (2013) 142–148.
[44] Microscale hierarchical three-dimensional flowerlike TiO2/PANI composite: synthesis, characterization, and its remarkable photocatalytic activity on organic dyes under UV-light and sunlight irradiation, J. Phys. Chem. C 118 (2014) 18343–18355.
[45] B. Samai, S.C. Bhattacharya, Conducting polymer supported cerium oxide nanoparticle: enhanced photocatalytic activity for waste water treatment, Mater. Chem. Phys. 220 (2018) 171–181.
[46] R. Djellabi, M.F. Ghorab, Photoreduction of toxic chromium using TiO_2-immobilized under natural sunlight: effects of some hole scavengers and process parameters, Desalin. Water Treat. 55 (2015) 1900–1907.
[47] L. Wu, S. Fang, L. Ge, C. Han, P. Qiu, Y. Xin, Facile synthesis of Ag@CeO_2 core–shell plasmonic photocatalysts with enhanced visible-light photocatalytic performance, J. Hazard. Mater. 300 (2015) 93–103.
[48] N. Wetchakun, S. Chaiwichain, B. Inceesungvorn, K. Pingmuang, S. Phanichphant, Andrew I. Minett, J. Chen, $BiVO_4$/CeO_2 nanocomposites with high visible-light-induced photocatalytic activity, ACS Appl. Mater. Interfaces 4 (2012) 3718–3723.
[49] B. Vellaichamy, P. Periakaruppan, Synergistic combination of a novel metal-free mesoporous band-gap-modified carbon nitride grafted polyaniline nanocomposite for decontamination of refractory pollutant, Ind. Eng. Chem. Res. 57 (2018) 6684–6695.